coatings

MDPI

Article

$MnNH_4P_2O_7$-Based Coating for High Temperature Assessment on the Surfaces of Cement Composites

Rajagopalan Sam Rajadurai [1], Jong-Han Lee [1,*], Eunsoo Choi [2] and Joo-Won Kang [3]

[1] Department of Civil Engineering, Inha University, Incheon 22212, Korea; samraj9593@gmail.com
[2] Department of Civil Engineering, Hongik University, Seoul 04066, Korea; eunsoochoi@hongik.ac.kr
[3] School of Architecture, Yeungnam University, Gyeongsan 38451, Korea; kangj@yumail.ac.kr
* Correspondence: jh.lee@inha.ac.kr; Tel.: +82-32-860-7564

Received: 28 February 2020; Accepted: 14 April 2020; Published: 17 April 2020



Abstract: This study examines the implementation of an $MnNH_4P_2O_7$ (ammonium manganese III pyrophosphate)-based coating on structural elements to obtain temperature information with color changes. Based on the $MnNH_4P_2O_7$ material, a coating was prepared and deposited on cement mortar surfaces. Heat experiments were then conducted to evaluate the thermochromism on the fabricated samples. The coated samples exhibited a superior irreversible thermochromic property at 400 °C with a color change from dark violet to light grayish blue at the heated surface. The color changes were retrieved at each temperature using a digital camera, and the change in color properties was evaluated in the *RGB* and *L*a*b** color spaces using image processing techniques. With increasing temperature from room temperature, the *RGB* values were almost constant until 200 °C. At higher temperatures, the color changes started to accelerate until 400 °C. The values showed a 167%, 567%, and 49% increase in *R*, *G*, and *B* values, respectively, at 400 °C. In the *L*a*b** color space, when the temperature was increased from room temperature to 400 °C, the *L*a*b** values showed an increase of 211%, a decrease of 94%, and an increase of 78%, respectively.

Keywords: ammonium manganese III pyrophosphate; coatings; inorganic pigment; temperature assessment; color change; imaging process

1. Introduction

Thermochromism is a phenomenon where the color changes as a response to variations in temperature. The color changes are based on the transition and/or transformation of the molecules when the materials are heated up or cooled. The materials can exist in different forms, such as metal oxides, polymers, solid-state semiconductors, and leuco-dyes [1,2]. Thermochromic materials can be classified as reversible and irreversible materials. Reversible thermochromic materials exhibit a shift in color when heated and a return to their original colors when cooled down to room temperature. These materials have been applied for solar reflectance in structures to provide a thermally comfortable indoor environment [3–7]. Kamalisarvestani et al. [8] proposed a thermochromic window coating that changes its color to block solar radiation. In addition, a temperature sensor based on a polydiacetylene material was proposed to show reversible color properties in solutions in response to temperatures between 30 and 70 °C [9]. Irreversible thermochromic materials experience a permanent color change at a certain temperature. Some studies were performed to utilize these materials as thermal indicating paints that can monitor the temperature change profiles and provide a damage warning on aero-engine components [10–12]. Moreover, Rabhiou et al. [13] proposed a phosphor-based irreversible thermal coating to measure the temperature in the range of 600 to 1000 °C. Most of the previous studies focused on temperature indicating systems on combustors used in gas turbine engines [14] and on the hot surfaces of metals [15]. On the other hand, few studies were designed to apply irreversible materials

in cement-based structures. Only Ma and Zhu [16] attempted to utilize a reversible thermochromic pigment in cement mortar that changes a color at a low temperature of 42 °C.

In concrete structures, the strength properties, mainly determined from the composition of concrete, change upon heating. When exposed to elevated temperature, concrete experiences physical and chemical changes, such as the evaporation of physically combined water, the dehydration of calcium silicate hydrate (CSH) and calcium hydroxide, and the decomposition of calcium carbonate and aluminates. With a normal concrete structure, a significant strength loss occurs between 300 and 600 °C [17]. The decrease in compressive strength commences from 300 °C, and the strength decreases by approximately 50% to 60% at 500 °C [18]. The tensile strength of a concrete slab exposed to 400 °C recovered 45% of its original strength and 40% of the residual bond strength obtained at room temperature [19,20]. Furthermore, the fatigue strength was not affected until the temperature reached 400 °C for concrete beams [21]. The color of concrete changes from normal to pink or red at temperatures ranging from 300 to 600 °C mainly due to the oxidation of iron components when using siliceous aggregate, but the color change is not obvious, particularly in concrete with calcareous and igneous aggregates [22,23]. In cement mortars, Yuzer et al. [24] evaluated the compressive strength and color change at high temperature. The strength loss started approximately at 300 °C, and the loss of the compressive strength accelerated above 300 °C. However, the color changes in cement mortars at high temperatures were visually unclear. Therefore, the beginning of this color change is difficult to recognize by the naked eye. The application of thermochromic materials on structural elements can provide temperature information with high resolution. Therefore, this study examined the color changes of an $MnNH_4P_2O_7$ material with increasing temperature.

Ammonium manganese III pyrophosphate, with the empirical formula $MnNH_4P_2O_7$, is a finely powdered inorganic pigment with earth abundant components. The $MnNH_4P_2O_7$ material is non-toxic and chemically stable with a typical dark violet, which has been used mainly in cosmetics, toys, and plastics [25]. The color of $MnNH_4P_2O_7$ has been reported to provide reversible color changes at 120 to 340 °C, which leads to an irreversible phase transition at 340 to 460 °C [26,27]. In this study, a thermochromic coating based on the $MnNH_4P_2O_7$ pigment was proposed to visualize high temperature variations accurately on the surface of cement-based materials with high spatial resolution.

Temperature measurements based on the above coatings provide a visual interpretation that further leads to an advanced process to measure color from the digital images [28]. The colors from the concrete surfaces can be measured using a range of instruments, such as a spectrophotometer, calibrated flatbed scanner, and digital camera [29,30]. A colorimetric analysis method was performed to take photographs under different light conditions, and the concrete colors were represented in the chromaticity diagram [31]. Furthermore, a study based on optical microscopy combined with color image analysis was conducted to quantify the changes in color for concrete subjected to elevated temperatures [32]. Digital cameras were also used to assess the surface color changes on siliceous concrete specimens [33–35]. Digital cameras are a desirable and suitable tool for data collection because the image quality has been markedly improved in recent years, and they are affordable and available. Digital images are generally recorded as three color (*RGB*) pixels. All colors are possibly expressed in cubic space [35]. Moreover, *RGB* values depend mostly on the instrument used to capture the image. Therefore, the *RGB* values are usually transformed to a standardized color space that is more suited for individual applications. The International Commission on Illumination (CIE) illustrates standardized color spaces. The CIE 1976 ($L^*a^*b^*$) color space is a standardized, device-independent, non-linear transformation of the *RGB* color space modelled with the human perception of color. The $L^*a^*b^*$ color space has linear measures of lightness (L^*) and two-color dimensions (a^* and b^*). The a^* dimension represents green (negative) to red (positive) intensities, and the b^* dimension represents a spectrum from blue (negative) to yellow (positive) [36].

This study utilizes $MnNH_4P_2O_7$-based coatings applied on the mortar surfaces to investigate the thermochromic color change and provide standardized color values. For this, heat experiments were performed to evaluate the thermochromic effects of $MnNH_4P_2O_7$ coatings. Digital images were

recorded from the surface at all temperatures. The color information of their respective images was analyzed using the *RGB* and *L*a*b** color spaces. The $MnNH_4P_2O_7$ coatings showed an irreversible color change at a high critical temperature that could be monitored using the color values in both *RGB* and *L*a*b** spaces.

2. Inorganic Color Changing Pigment

Ammonium manganese III pyrophosphate is a finely powdered inorganic material with a chemical formula, $MnNH_4P_2O_7$. Table 1 shows the characteristics of $MnNH_4P_2O_7$ pigment manufactured at Kremer Pigmente in Germany, which is composed of earth abundant components, such as manganese dioxide, ammonium dihydrogen phosphate, and phosphoric acid [26,37]. The dark violet color of the inorganic material is due to the presence of phosphate and ammonia; the material is insoluble in organic and most ionic solvents. Figure 1a displays the dark violet color of the pigment at room temperature.

Table 1. Typical characteristics of $MnNH_4P_2O_7$ pigment [26].

Parameter	Characteristics
Color	Dark violet
Chemical characterization	Ammonium manganese III pyrophosphate
Density	2.7–2.9 kg/m^3
Bulk density	0.60 g/cm^3
Average particle size	2.30 µm
pH value	2.5–4.7
Thermal decomposition	>400 °C



(**a**) (**b**) (**c**)

Figure 1. Color change of $MnNH_4P_2O_7$ pigment: (**a**) room temperature; (**b**) 370 °C; (**c**) 410 °C.

When heated to 370 °C from room temperature, the pigment particles changed from dark violet to reversible blue color, as shown in Figure 1b. At the discoloration temperature, the H_2O molecules are driven off from the particles, which leads to the change in $Mn_2P_4O_{13}(NH_3)_2$ and blue color as expressed in Equation (1). When exposed to the room atmosphere, $Mn_2P_4O_{13}(NH_3)_2$ reacts with atmospheric moisture and returns to the original dark violet color [27].

At the higher temperature of 410 °C, the particles experience an irreversible color change to grayish yellow, as shown in Figure 1c. The application of further heat to the pigment causes the liberation of NH_3 from the particles, which is associated with the oxidation of hydroxylamine to change $Mn_2P_4O_{13}(NH_3)_2$ to $Mn_2P_4O_{12}$ (manganous tetra-metaphosphate), as described in Equation (2). Then, the oxidized hydroxylamine (NH_3OH) is broken into nitrogen (N_2) and water (H_2O), or the ammonia (NH_3) is directly oxidized to nitrogen [27]. When cooled to room temperature, the particles retain the grayish yellow color and do not recover the original color.

$$\underset{\text{(Ammonium manganese (III) pyrophosphate)}}{2MnNH_4P_2O_7} \xrightarrow{-H_2O} Mn_2P_4O_{13}(NH_3)_2 \quad (1)$$

$$Mn_2P_4O_{13}(NH_3)_2 \xrightarrow[-NH_3]{-NH_3OH \rightarrow N_2 + H_2O} Mn_2P_4O_{12} \quad \text{(Manganous tetra metaphosphate)} \tag{2}$$

3. Experiments

3.1. Preparation of Specimens and Test Variables

The following procedures were followed to prepare the specimens, resembling the application of coatings in real buildings. Sample preparation consisted of two stages. The first stage involved the preparation of coating surfaces, and the second stage included the preparation of coatings and fabrication.

Cement mortar samples, $50 \times 50 \times 50$ mm^3 in size, were prepared by mixing water, silica sand, and ordinary Portland cement (Type I), manufactured at a local company. The ratios of water to cement and sand to cement were 0.4 and 2, respectively. The prepared specimens were left under cover inside the laboratory for 24 h. They were then removed from the molds and cured in water in a constant temperature and humidity chamber (20 ± 2 °C, 60% ± 10%) until the test. Subsequently, the mortar specimens were dried for 24 h at 100 °C in an oven.

Figure 2 shows the coating procedure on a cross section of the specimens. The mortar surfaces were cleaned using sandpaper, and the dust and dirt particles were removed to maintain a clean surface and allow adhesion of the applied coating to the mortar surface, as shown in Figure 3a. The first coating, called the prime coating, was dropped on the surface with silica-based binder and water at a 1:5 ratio. The prime coated samples were placed in an oven at 100 °C for 10 min and dried for 6 h at ambient temperature, as shown in Figure 3b. To prepare the coating solution, pigment and water were added at a 2:3 ratio and stirred for 10 min at room temperature with the slow addition of 10% silica-based binder under stirring. Finally, the coating solution was poured on the specimen surface and coated in a single layer, as shown in Figure 3c. The coated surfaces were left undisturbed at room temperature for seven days to cure and achieve complete color exposure on the surfaces. After curation, the specimens were placed in a furnace chamber and heated to the target temperatures of 100, 200, 300, 400, and 450 °C. At each target temperature, the specimen was maintained for around 30 min and taken out to photograph the surface of the specimen using a digital camera. After that, the specimen was placed again in the furnace and heated to the next target temperature.

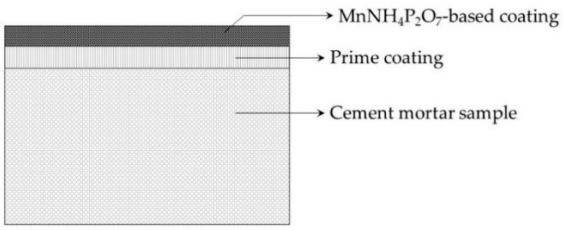

Figure 2. Cross section of the coatings on the surface.



(**a**) (**b**) (**c**)

Figure 3. Specimens and coatings on the surface: (**a**) mortar surface; (**b**) prime coating; (**c**) $MnNH_4P_2O_7$-based coating.

3.2. Image Acquisition and Post Processing

The color data were collected by photographing the surfaces at all temperature intervals. A digital camera (ILCE-TR, SONY, Tokyo, Japan) with a 7360 × 4912-pixel resolution was placed at a fixed position, approximately 30 cm above the specimens. All the images were recorded using the highest pixel count (most pixels per object area) to provide high quality images. The recorded photographs were imported to a computer and analyzed using an image processing technique. The color and brightness of the light source have a significant influence on the color of the surface. Photographs were taken in a consistent illuminance throughout at all temperatures to minimize the variation in color and brightness.

The color of the images on the surface of the samples was analyzed using MATLAB Version 9.6 programming to extract the *RGB* and *L*a*b** color information. From the images obtained at different temperatures, the surfaces of the samples were taken from the background as the regions of interest, as shown in Figure 4a. That is, the sample surface of approximately 1000 × 1000 pixels was separated from the total image (7360 × 4912 pixels). Then, the mean and standard deviation of the *RGB* and *L*a*b** color values were obtained from the separated sample surface at each pixel. Furthermore, the separated surface was divided into 4 × 4 regions to present more accurate color values, as shown in Figure 4b. The mean and standard deviation of *RGB* and *L*a*b** color values were also calculated using the separate 4 × 4 regions defined as approximately 250 × 250 pixels for each region.

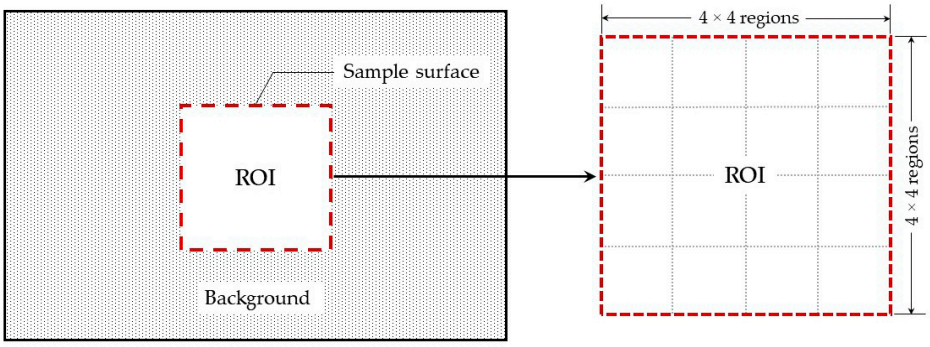

Figure 4. Selections of the region of interest (ROI): (**a**) ROI extracted from the background; (**b**) ROI divided into 4 × 4 regions.

Each color in the *RGB* space is represented by a combination of spectral components of red, green, and blue colors. The values of each *RGB* component are in the range 0 to 255. The measured *RGB* color values are related to the lighting conditions (color and brightness), colors of the objects being recorded, and the sensitivity of the recording image sensor. Thus, the *RGB* color space used in digital cameras is device-dependent. The color values of the pigment can correspond to predefined values of the ColorHexa codes. Hence, the captured images were adjusted by changing the illumination and settings of the camera to match the predefined ColorHexa codes [38,39]. ColorHexa is a six-digit color code providing information about the colors obtained from the images [40]. Therefore, to compensate for the variations due to the color and brightness of the light source, the *RGB* images were transformed into standardized, device-independent CIE1976 (*L*a*b**) space using MATLAB programming. This resulted in values between 0 and 100 for the *L** dimension, and −128 and 128 for *a** and *b** dimensions.

4. Results and Discussion

4.1. Thermal Response of Cement Composites and $MnNH_4P_2O_7$-Based Coatings with Temperatures

$MnNH_4P_2O_7$-based inorganic coatings were applied to a cement mortar specimen using pigment coating formulations and curing conditions. Figure 5 presents the surface color of the mortar specimen

without the $MnNH_4P_2O_7$ coating. At room temperature, the surface color of the cement mortar exhibited a dark grayish color, as shown in Figure 5a. With increasing temperature, the surface color was very similar to the dark grayish color presented at room temperature. At high temperatures between 300 and 450 °C, the surface color of the mortar was slightly darkened, as shown in Figure 5d–f, but no significant color changes were observed by naked eye.

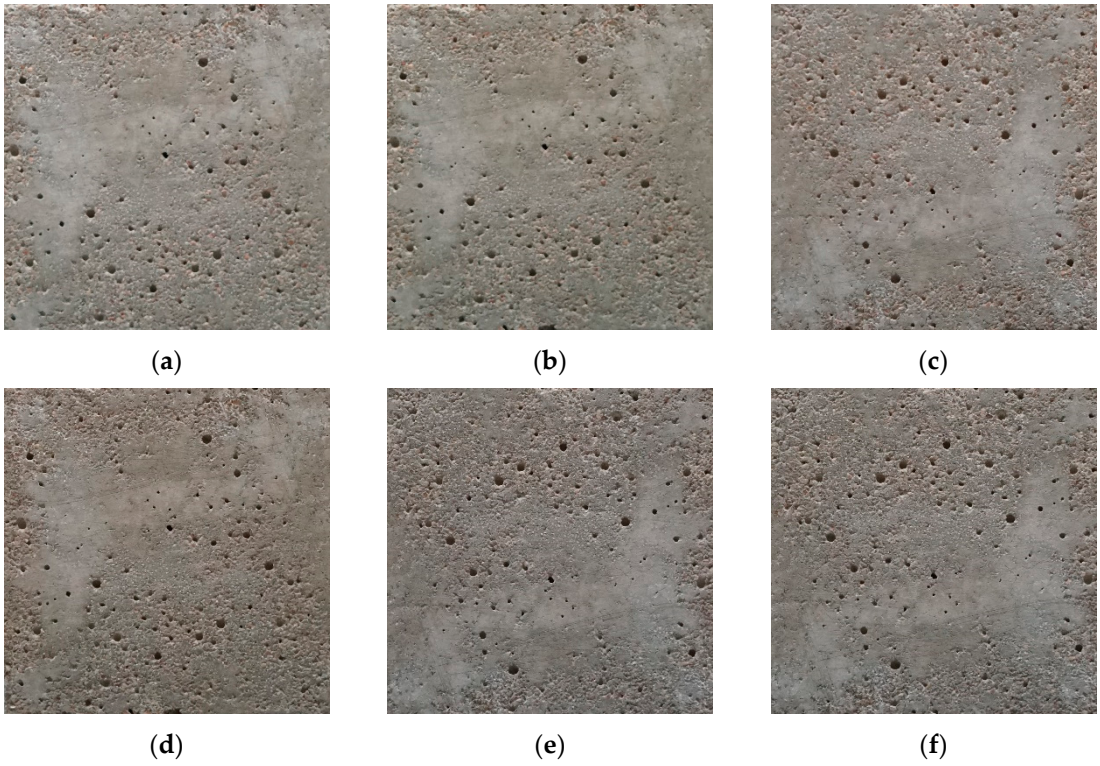

Figure 5. Surface colors of the mortar specimen without $MnNH_4P_2O_7$ coating at (**a**) ambient temperature; (**b**) 100 °C; (**c**) 200 °C; (**d**) 300 °C; (**e**) 400 °C; (**f**) 450 °C.

The thermochromic behavior of the $MnNH_4P_2O_7$ coating on the mortar is shown in Figure 6. The mortar sample coated with the $MnNH_4P_2O_7$ coating showed a dark violet color at ambient temperature, as illustrated in Figure 6a. Figure 6b,c show samples at 100 and 200 °C, respectively. At 100 °C, the coating sample displayed the same dark violet color observed at ambient temperature. At 200 °C, the sample exhibited a very dark, desaturated blue color. This was attributed to the evaporation of water particles, due to heating, moving towards the outer surface of the mortar specimen due to the increase in temperature. Figure 6d shows the sample heated to 300 °C, at which the violet-pattern color on the surface disappeared. That is, the color of the coating changed from very dark desaturated blue to grayish violet with the evaporation of water particles. As the temperature was increased to 400 °C, the surface coating displayed excellent thermochromic progress and turned to light grayish blue. The coatings achieved an extensive, irreversible color change at 400 °C, which was 10 °C lower than the temperature observed for the pigment. This might be due to the occurrence of pigments dispersed in the coating, which was manufactured by a 2:3 pigment-to-water ratio. Further heating to 450 °C resulted in a stable light grayish blue color. Figure 6e,f show the color changes of the samples with a $MnNH_4P_2O_7$ coating at 400 °C and 450 °C, respectively. After cooling to room temperature, the samples retained the changed light grayish blue color, indicating irreversible thermochromic behavior. When applied to the surface of the concrete structures, the thermochromic $MnNH_4P_2O_7$ coatings developed in the laboratory can provide a tool to determine the temperature, with a change in color defined as a function of temperature.

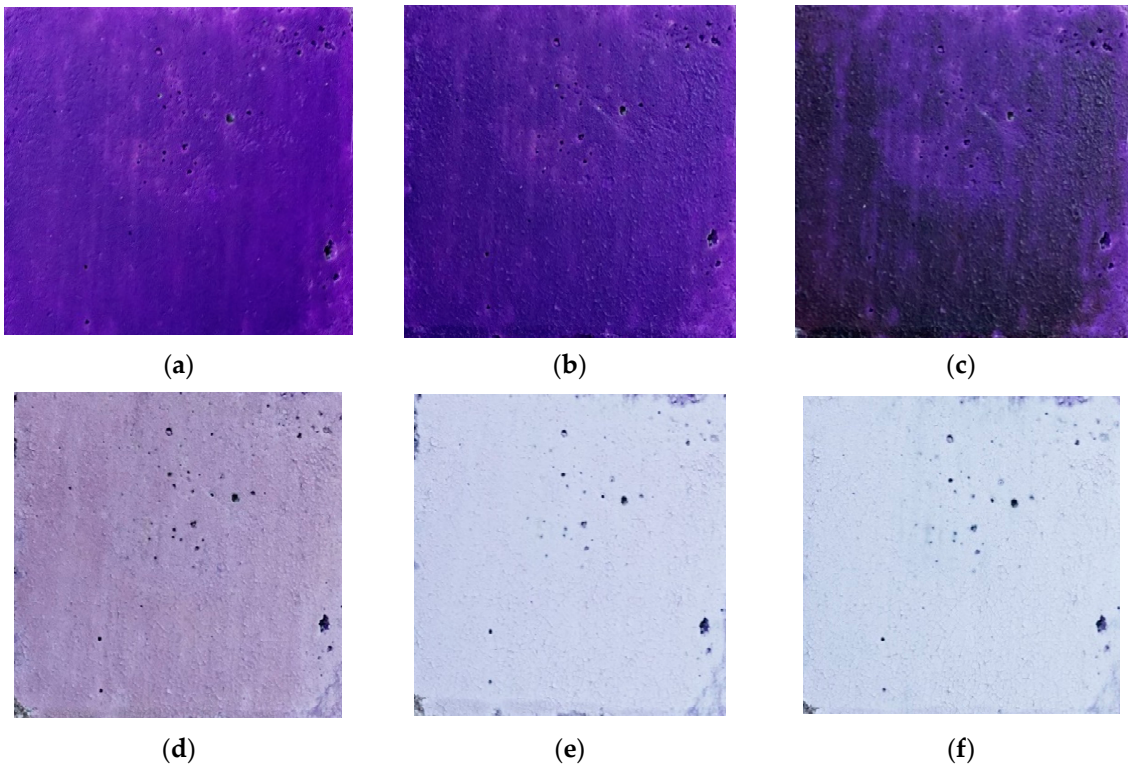

Figure 6. Color change process of $MnNH_4P_2O_7$ coating obtained at (**a**) ambient temperature; (**b**) 100 °C; (**c**) 200 °C; (**d**) 300 °C; (**e**) 400 °C; (**f**) 450 °C.

4.2. Color Changes Obtained in the RGB Color Space from Digital Images with Temperatures

Figure 7 presents the changes in the *RGB* values on the surfaces of the mortar specimen. With increasing temperature from room temperature, the mean *RGB* values were around (141, 136, 129) indicating dark grayish orange (Hex code #8d8881), and they were almost invariant until 200 °C. The *RGB* values decreased by 8%, 9%, and 11% at 300 °C to show the mean (124, 118, 109), respectively, corresponding to dark grayish orange (Hex code #7c766d). After that, the RGB values exhibited relatively similar values of (123, 119, 113) at 400 °C and (123, 118, 113) at 450 °C, which correspond to dark grayish orange (Hex codes #7b7771 and #7b7671, respectively). The cement mortar with some pores on the surface provided some variations in the *RGB* values, which led to the standard deviation in the range of 20 to 24.

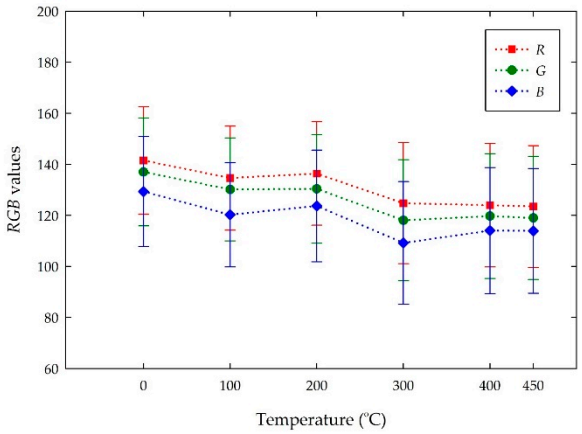

Figure 7. Color changes and their standard deviations of the mortar surfaces obtained in *RGB* values.

The quantitative difference of colors on the surface of the coating samples at ambient temperature and those at critical temperature when the color completely changed were analyzed using the images obtained at each temperature. The variation in the thermochromic color of the coating samples with increasing temperature was expressed in three-dimensional *RGB* color space. The mean and standard deviation of the *RGB* values were calculated at each pixel from the sample surfaces. Figure 8 presents the *RGB* mean values with the standard deviation obtained from the surfaces with increasing temperature. The mean *RGB* values were interpreted to determine their corresponding ColorHexa codes and color description at various temperatures, as shown in Table 2.

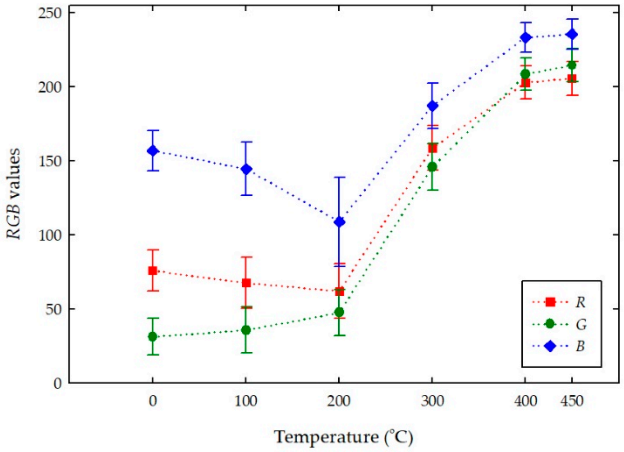

Figure 8. Color changes and their standard deviations of the coating surface obtained in *RGB* values.

Table 2. Coatings—*RGB* color change values and their corresponding color charts.

Temperature (°C)	Color Values			Hex Code	Color Description
	Red (*R*)	Green (*G*)	Blue (*B*)		
Room Temperature	76 ± 13	31 ± 12	157 ± 13	#4b1f9c	Dark violet
100	67 ± 17	35 ± 15	144 ± 18	#432390	Dark violet
200	62 ± 18	47 ± 15	109 ± 30	#3d2f6c	Dark desaturated blue
300	159 ± 15	146 ± 15	187 ± 15	#9E91BB	Grayish violet
400	202 ± 11	209 ± 11	233 ± 10	#cad0e9	Light grayish blue
450	205 ± 11	214 ± 11	235 ± 10	#cdd6eb	Light grayish blue

The *RGB* values at ambient temperature were (76, 31, 157), which represent a dark violet color (Hex code #4b1f9c). These values were relatively constant and stable until 200 °C. As the temperature was increased to 300 °C, the *RGB* values increased to (159, 146, 187), and the color changed to grayish violet (Hex code #9E91BB). At 400 °C, the thermochromic coating lost its chroma and transformed from dark to light grayish blue (Hex code #cad0e9) with an increase in all the *RGB* values to (202, 209, 233). Compared to those at room temperature, the *RGB* values increased by approximately 167%, 567%, and 49%, respectively. Few changes in the *RGB* values were observed when the temperature was increased to above 400 °C. The standard deviations of the *RGB* values, as shown in Figure 8, were in the range of 13 to 30 from room temperature to 200 °C. The deviations of the *RGB* values revealed some variations at each pixel of the image mainly due to uneven coatings and some pores on the surface. After the coating surface changed completely to light grayish blue at 400 °C, the deviations were relatively low, in the range of 10 to 11.

The images were divided into 4 × 4 regions on the surface, and the mean *RGB* values were extracted over the divided regions. The values extracted at 4 × 4 regions were plotted in the three-dimensional diagrams shown in Figure 9. Figure 9 represents a surface plot of the *RGB* values at room temperature and 400 °C. The mean *R* values obtained over 4 × 4 regions were between 60 and 93 at room temperature and 200 and 207 at 400 °C. The mean *G* values in the 4 × 4 regions were between 17 and 47 at room

temperature and between 205 and 211 at 400 °C. The *B* values at room temperature in the 4 × 4 regions ranged from 142 to 176, and from 231 to 236 at 400 °C. As discussed with respect to the standard deviations, the *RGB* values obtained in 4 × 4 regions had some variations at room temperature but similar values at 400 °C. Some changes at room temperature might have been due to variations in the coating density of the dark and light particles on the relatively small surface. At 400 °C, the color change was obtained uniformly throughout the surface, which minimized the variations.

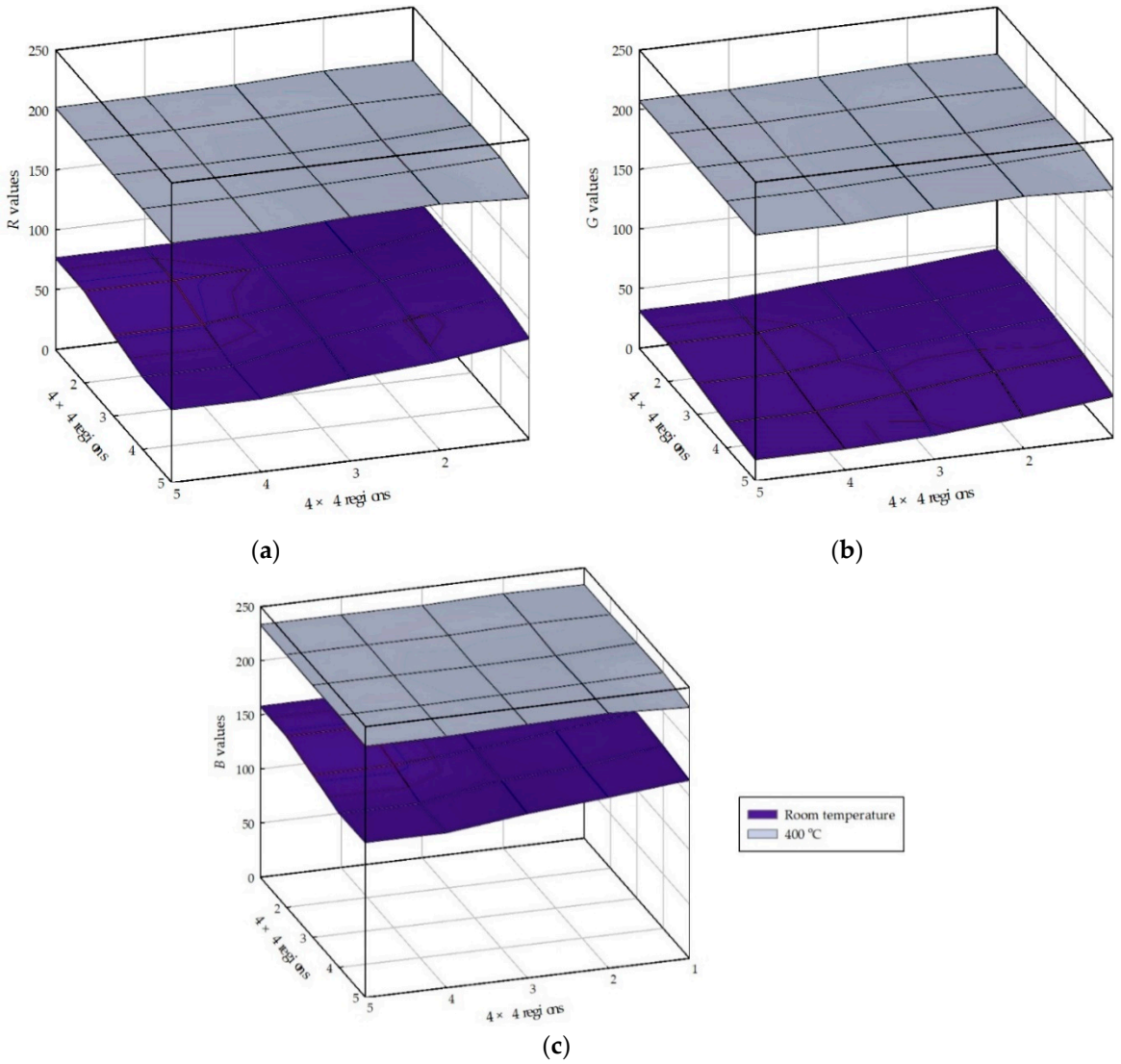

Figure 9. Color intensities in 4 × 4 regions on the surface: (**a**) *R* values; (**b**) *G* values; (**c**) *B* values.

In addition, this study analyzed the total color changes of the mean *RGB* values obtained at room temperature and 400 °C. The total color change is defined as the Euclidean distance (ΔD) in the *RGB* color space shown in Equations (3)–(6)

$$\Delta D = \sqrt{(\Delta R^2 + \Delta G^2 + \Delta B^2)} \quad (3)$$

$$\Delta R = R_2 - R_1 \quad (4)$$

$$\Delta G = G_2 - G_1 \quad (5)$$

$$\Delta B = B_2 - B_1 \quad (6)$$

where ΔR, ΔG, and ΔB represent the color changes, in which R_1, G_1, and B_1 are the mean values at room temperature, and R_2, G_2, and B_2 are the mean values at 400 °C. The total color change ΔD showed an increase of intensities from room temperature to 400 °C, at which point ΔD reached approximately 231.

*4.3. Color Changes Obtained in the L*a*b* Color Space from Digital Images with Temperatures*

The *RGB* images obtained were converted to CIE 1976 (*L*a*b**) color space to provide more standardized results. The lightness (*L**) is given a value of 100 for white and 0 for ideal black. The *a** and *b** parameters are in the range of −128 and 128; *a** indicates greenness and redness, respectively, and *b** indicated blueness and yellowness, respectively. Figure 10 presents the changes in the *L*a*b** values on the mortar surface with increasing temperature. The *L*a*b** values at room temperature were (57, 0.2, 4), which remained almost constant until 200 °C. At 300 °C, a slight decrease and increase in the *L** and *a** values was obtained to show the *L*a*b** values of (49, 0.9, 5). At the temperatures of 400 °C and 450 °C, the *L*a*b** values were very similarly (50, 0.6, 4) and (50, 0.7, 4), respectively. Thus, little change was found in the *L*a*b** values on the surfaces of the mortar specimen with increasing temperature. The deviations obtained in the *L** value were in the range of 8 to 9, and those in the *a** and *b** values were in the range of 1 to 2.

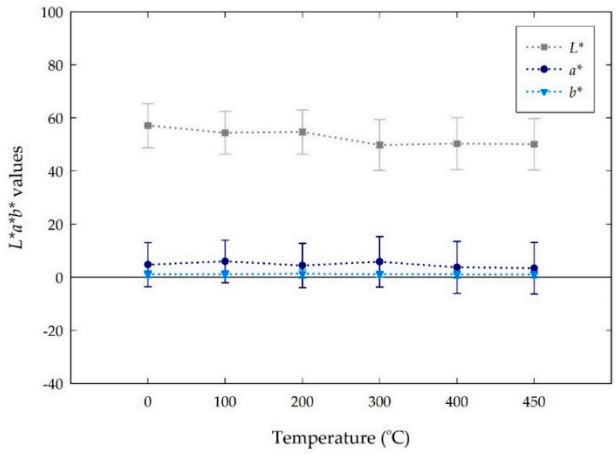

Figure 10. Color changes on the mortar surfaces obtained in *L*a*b** values.

Figure 11 presents the changes on the coating surface in the *L*a*b** values with increasing temperatures. The mean and standard deviation of the *L*a*b** values and their corresponding color charts are also summarized in Table 3. The mean *L** value at room temperature was 26, which represents a dark appearance. The value remained relatively constant up to 200 °C. As the temperature was increased further to 300 °C, the *L** value increased to 62. At 400 °C, the *L** value rapidly increased to 84, and the color completely changed to a light color. Compared to that at room temperature, the *L** value at 400 °C increased by 211%. The mean *a** and *b** values at room temperature were 48 and −60, respectively, which means redness (+*a**) and blueness (−*b**). From the temperature of 200 °C, the *a** value gradually decreased with a concomitant increase in *b** value. Compared to the *a** and *b** values at room temperature, the *a** value at 400 °C decreased by 94% to a value of 2, and the *b** value at 400 °C increased by 78% to −12. The standard deviations were also obtained at all pixels in the images at all temperatures. The standard deviations of the *L*a*b** values between room temperature until 300 °C ranged from 5 to 8, 2 to 9, and 2 to 11, respectively. When the temperature reached more than 400 °C, the deviations of the *L** values were in the range of 5 to 6, whereas those of the *a** and *b** values were in the range of 1 to 2. This means that the color change obtained at the critical temperature of 400 °C was uniform over the entire coating surface, which showed relatively small deviations.

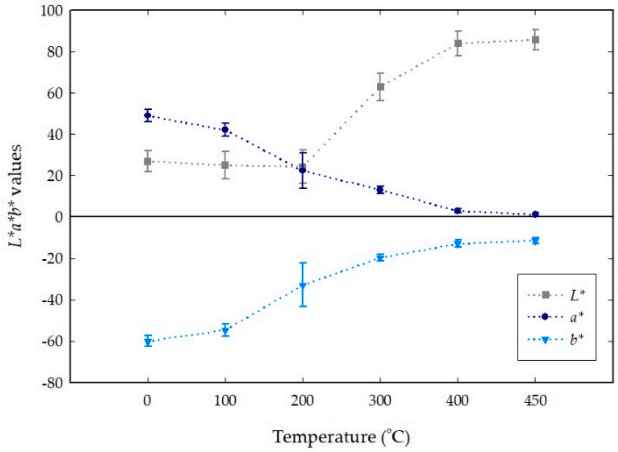

Figure 11. Color changes on the coating surfaces obtained in $L^*a^*b^*$ values.

Table 3. Coatings—$L^*a^*b^*$ color change values and their corresponding color charts.

Temperature (°C)	Color Values			Hex Code	Color Description
	L^*	a^*	b^*		
Room Temperature	26 ± 5	48 ± 3	−60 ± 2	#4b1f9c	Dark violet
100	25 ± 6	42 ± 3	−54 ± 3	#432390	Dark violet
200	24 ± 8	22 ± 8	−32 ± 10	#3d2f6c	Dark desaturated blue
300	62 ± 6	13 ± 1	−19 ± 1	#9E91BB	Grayish violet
400	83 ± 5	2 ± 1	−12 ± 1	#cad0e9	Light grayish blue
450	85 ± 4	1 ± 1	−11 ± 1	#cdd6eb	Light grayish blue

Moreover, the images were extracted into 4 × 4 regions, and the $L^*a^*b^*$ information was analyzed, as shown in Figure 12. In Figure 12a, the mean L^* values in the 4 × 4 regions were in the range of 22 to 33 at room temperature and 83 to 84 at 400 °C. The mean a^* values obtained at room temperature were between 47 and 51 in the 4 × 4 regions, and those at 400 °C were between 2 and 3, as shown in Figure 12b. The mean b^* values obtained in the 4 × 4 regions ranged from −61 to −58 at room temperature and −13 to −12 at 400 °C, as shown in Figure 12c.

The total color changes were also calculated based on the $L^*a^*b^*$ values using Equations (7)–(10).

$$\Delta D^* = \sqrt{(\Delta L^*)^2 + (\Delta a^*)^2 + (\Delta b^*)^2} \quad (7)$$

$$\Delta L^* = L_2^* - L_1^* \quad (8)$$

$$\Delta a^* = a_2^* - a_1^* \quad (9)$$

$$\Delta b^* = b_2^* - b_1^* \quad (10)$$

where $L_1{}^*$, $a_1{}^*$, and $b_1{}^*$ represent the color values at room temperature, and $L_2{}^*$, $a_2{}^*$, and $b_2{}^*$ represent the values at 400 °C. With $\Delta L^* = 57$ of the coating surfaces indicating a light color, the change in a^*, i.e., Δa^*, was −46, indicating a light shade of green. The change in b^*, i.e., Δb^*, was 47, indicating a light shade of yellow. Thus, the total color change ΔD^* of the coating surface was approximately 87.

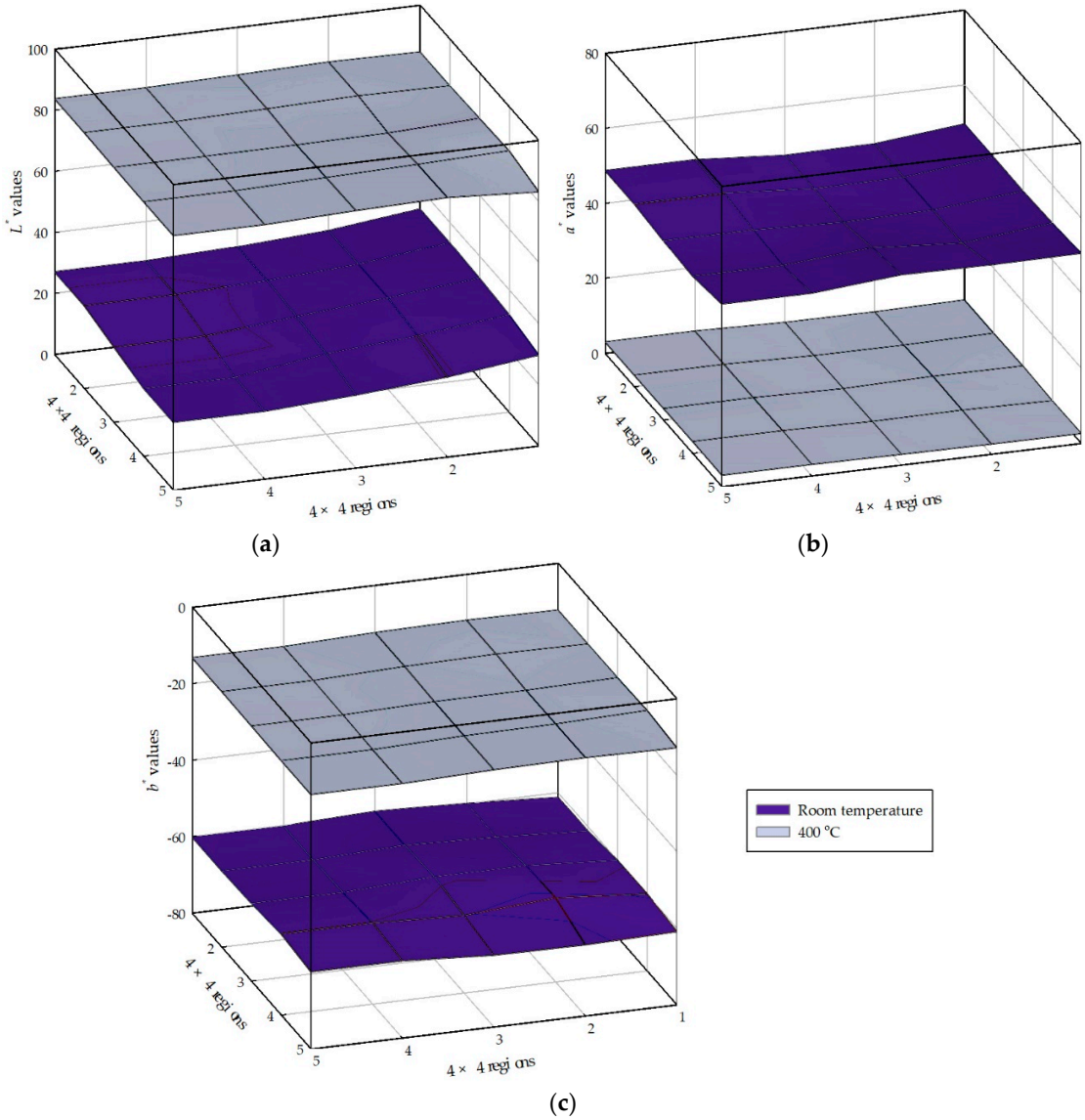

Figure 12. Color intensities in 4 × 4 regions on the surface: (**a**) *L** values; (**b**) *a** values; (**c**) *b** values.

5. Summary

The fabricated samples with the $MnNH_4P_2O_7$-based coating were found to respond to increasing temperature. Up to 100 °C, the coating sample displayed the same dark violet color obtained at ambient temperature. As the temperature was increased to 200 °C, the sample showed a very dark desaturated blue color mainly due to the evaporation of water particles. The violet-pattern color disappeared and changed to grayish violet at 300 °C. At 400 °C, the coating surface completely turned to light grayish blue. Further heating to higher temperatures and cooling to room temperature resulted in a stable light grayish blue color, which indicates irreversible thermochromic behavior.

The *RGB* values at ambient temperature, which represent a dark violet color, were almost constant and stable to 200 °C. At 400 °C, when the thermochromic coating lost its darkness and completely changed to light grayish blue, the *RGB* values increased by 167%, 567%, and 49%, respectively. The *RGB* values also exhibited relatively small deviations at 400 °C, which means that a relatively uniform color change was achieved throughout the entire surface. The total change in the *RGB* values, which is defined as the Euclidean distance, showed an increasing trend with increasing temperature and reached approximately 231 at a critical temperature of 400 °C. A small change in the *RGB* values was obtained when the temperature was increased to above 400 °C.

In the $L^*a^*b^*$ color space, the L^* value was essentially dark at room temperature but rapidly increased toward the lightness intensity at 400 °C. The a^* and b^* values demonstrated rich redness and blueness, respectively, at room temperature. The $L^*a^*b^*$ values at room temperature remained relatively constant up to 200 °C. At 400 °C, when the coating surface completely turned to light grayish blue, the L^* and b^* values at 400 °C increased by 211% and 78%, respectively, and the a^* decreased by approximately 94%. Similar to those of the *RGB* values, the standard deviations of the $L^*a^*b^*$ values were also relatively small, indicating that the color change obtained at a critical temperature of 400 °C was uniform over the entire coating surface. The total change in the $L^*a^*b^*$ values of the coating from the room temperature to the critical temperature of 400 °C was approximately 87.

6. Conclusions

This study presented a method for the quick and exact assessment of the temperature profiles after an abnormally high temperature was applied to a structure element. A thermochromic coating based on $MnNH_4P_2O_7$ was fabricated and successfully applied to the mortar surface. The applied coating provided the excellent color changing process from dark violet to light grayish blue when heated to 400 °C. In addition to the change in the visual color, the color properties in the *RGB* and $L^*a^*b^*$ spaces were evaluated as a function of temperatures.

This study successfully demonstrated the feasibility and applicability of the thermochromic $MnNH_4P_2O_7$ coating as a temperature detection technology. When applied to cementitious materials and structures, the thermochromic $MnNH_4P_2O_7$ coating could provide a tool for determining the temperature information with the color information defined as a function of temperature. In addition, the results of the study indicate that the developed coating holds great potential for applications in electric appliances, jet engines, and automotive sectors in areas of research and development, maintenance, and non-destructive testing.

Author Contributions: R.S.R., J.-H.L., E.C., and J.-W.K. designed and planned the experiments; R.S.R. performed the experiments; J.-H.L., E.C., and J.-W.K. analyzed the data; R.S.R. and J.-H.L. wrote and revised the paper. All authors have read and agreed to the published version of the manuscript.

Funding: This research was supported by a grant from the Mid-Career Research Program (NRF-2019R1A2C1006494) through the National Research Foundation (NRF) Korea.

Conflicts of Interest: The authors declare no conflict of interest.

References

1. Ferrara, M.; Bengisu, M. Materials That Change Color. In *Springer Briefs in Applied Sciences and Technology*; Springer Science and Business Media LLC: Heidelberg, Germany, 2013.
2. Jorgensen, G. *Electrochromic and Thermochromic Materials for Solar Energy Applications with Emphasis on Niobium and Vanadium Oxides*; University of California: Berkeley, CA, USA, 1984.
3. Ma, Y.; Zhu, B.; Wu, K. Preparation and solar reflectance spectra of chameleon-type building coatings. *Sol. Energy* **2001**, *70*, 417–422.
4. Zheng, S.; Xu, Y.; Shen, Q.; Yang, H. Preparation of thermochromic coatings and their energy saving analysis. *Sol. Energy* **2015**, *112*, 263–271. [CrossRef]
5. Apostolakis, K.; Karlessi, T.; Santamouris, M.; Didaskalopoulos, P.; Synnefa, A.; Assimakopoulos, D. Development and testing of PCM doped cool colored coatings to mitigate urban heat island and cool buildings. *Build. Environ.* **2010**, *46*, 570–576.
6. Apostolakis, K.; Karlessi, T.; Synnefa, A.; Livada, I.; Santamouris, M. Development and testing of thermochromic coatings for buildings and urban structures. *Sol. Energy* **2008**, *83*, 538–551.
7. Saliari, M.; Papantoniou, S.; Santamouris, M.; Kolokotsa, D.; Vangeloglou, E.; Karlessi, T.; Maravelaki-Kalaitzaki, P. Development and analysis of mineral based coatings for buildings and urban structures. *Sol. Energy* **2012**, *86*, 1648–1659.
8. Kamalisarvestani, M.; Saidur, R.; Mekhilef, S.; Javadi, F.S. Performance, materials and coating technologies of thermochromic thin films on smart windows. *Renew. Sustain. Energy Rev.* **2013**, *26*, 353–364. [CrossRef]

9. Chen, X.; Yoon, J. A thermally reversible temperature sensor based on polydiacetylene: Synthesis and thermochromic properties. *Dye. Pigment.* **2011**, *89*, 194–198. [CrossRef]
10. Yang, L.; Li, Z.M. The research of temperature indicating paints and its application in aero-engine temperature measurement. *Procedia Eng.* **2015**, *99*, 1152–1157. [CrossRef]
11. Lempereur, C.; Andral, R.; Prudhomme, J.Y. Surface temperature measurement on engine components by means of irreversible thermal coatings. *Meas. Sci. Technol.* **2008**, *19*, 105501. [CrossRef]
12. Popescu, M.; Serban, L.; Popescu, M. Thermo-indicating paint for damage warning. *J. Therm. Anal. Calorim.* **1996**, *46*, 317–321. [CrossRef]
13. Rabhiou, A.; Feist, J.; Kempf, A.; Skinner, S.; Heyes, A. Phosphorent thermal history sensors. *Sens. Actuators A Phys.* **2011**, *169*, 18–26. [CrossRef]
14. Arulprakasajothi, M.; Rupesh, P.L. Surface temperature measurement of gar turbine combustor using temperature-indicating paint. *Int. J. Amb. Energy* **2020**. [CrossRef]
15. Rupesh, P.L.; Arulprakasajothi, M. Thermal history analysis on a hot surface using temperature indicating paints. *Int. J. Amb. Energy* **2020**. [CrossRef]
16. Ma, Y.; Zhu, B. Research on the preparation of reversibly thermochromic cement based materials at normal temperature. *Cem. Concr. Res.* **2009**, *39*, 90–94. [CrossRef]
17. Lee, J. The effect of high temperature on color and residual compressive strength of concrete. In Proceedings of the 7th international Conference on Fracture Mechanics of Concrete and Concrete Structures. High Performance, Fiber Reinforced Concrete, Special Loadings and Structural Applications, Jeju, Korea, 23–28 May 2010; pp. 1772–1775.
18. Hager, I. Behaviour of cement concrete at high temperature. *Bull. Polish Acad. Sci. Tech. Sci.* **2013**, *61*, 1–10. [CrossRef]
19. Hajiloo, H.; Green, M.F. Post-fire residual properties of GFRP reinforced concrete slabs: A holistic investigation. *Compos. Struct.* **2018**, *201*, 398–413. [CrossRef]
20. Yu, B.; Kodur, V.K.R. Effect of high temperature on bond strength of near-surface mounted FRP reinforcement. *Compos. Struct.* **2014**, *110*, 88–97. [CrossRef]
21. Zhao, J.; Li, G.; Wang, Z.; Zhao, X.L. Fatigue behavior of concrete beams reinforced with glass- and carbon-fiber reinforced polymer (GFRP/CFRP) bars after exposure to elevated temperatures. *Compos. Struct.* **2019**, *229*, 111427. [CrossRef]
22. Annerel, E.; Taerwe, L. Revealing the temperature history in concrete after fire exposure by microscopic analysis. *Cem. Concr. Res.* **2009**, *39*, 1239–1249. [CrossRef]
23. Hager, I. Colour change in heated concrete. *Fire Technol.* **2014**, *50*, 945–958. [CrossRef]
24. Yuzer, N.; Akoz, F.; Ozturk, D.L. Compressive strength–color change relation in mortars at high temperature. *Cem. Concr. Res.* **2004**, *34*, 1803–1807. [CrossRef]
25. Begum, Y.; Wright, A.J. Relating highly distorted Jahn-Teller MnO_6 to colouration in manganese violet pigments. *J. Mater. Chem.* **2012**, *22*, 21110–21116. [CrossRef]
26. Rajagopalan, S.R.; Lee, J.H. High temperature sensing and detection for cementitious materials using manganese violet pigment. *Materials* **2020**, *13*, 993.
27. Lee, J.D.; Browne, L.S. The nature and properties of manganese violet. *J. Chem. Soc. A* **1968**, 559–561. [CrossRef]
28. Liu, T.; Sullivan, J.P. Pressure and Temperature Sensitive Paints. In *Technology and Engineering*; Springer: Berlin, Germany, 2019; Volume 53.
29. Annerel, E.; Taerwe, L. Methods to quantify the colour development of concrete exposed to fire. *Constr. Build. Mater.* **2011**, *25*, 3989–3997. [CrossRef]
30. Felicetti, R. Digital camera colorimetry for the assessment of fire damaged concrete. In Proceedings of the International Conference on Fire deign of Concrete Structures: What now? What next? Milan, Italy, 2–4 December 2004.
31. Wei, Y.; Kong, W.K.; Wan, C.; Wang, Y.Q. The colorimetry method in assessing fire-damaged concrete. *J. Adv. Concr. Technol.* **2019**, *17*, 282–294. [CrossRef]
32. Short, N.R.; Guise, S.E.; Purkiss, J.A. Assessment of fire damaged concrete using colour image analysis. *Constr. Build. Mater.* **2001**, *15*, 9–15. [CrossRef]
33. Annerel, E.V.; Taerwe, L.R. Assessment techniques for the evaluation of concrete structures after fire. *J. Struct. Fire Eng.* **2013**, *4*, 123–130.

34. Felicetti, R. Combined while-drilling techniques for the assessment of deteriorated concrete cover. In Proceedings of the 7th International Symposium on Nondestructive Testing in Civil Engineering, Nantes, France, 30 June–3 July 2009.
35. Tkaleie, M.; Tasie, J.F. *Color Spaces—Perceptual, Historical and Applicational Background*; IEEE: Ljubljana, Slovenia 2003; pp. 304–308.
36. Kheng, L.W. Color spaces and color-difference equations. *Color Res. Appl.* **2002**, *24*, 186–198.
37. MnNH4P2O7. Available online: https://www.kremer-pigmente.com (accessed on 1 January 2018).
38. Pascale, D. *RGB Coordinates of the Macbeth Color Checker*; Babel Color Co.: Montreal, Canada, 2006; pp. 1–16.
39. RGB Tables. Available online: https://www.rapidtables.com/web/color/RGB_Color.html (accessed on 1 November 2019).
40. ColorHexa. Available online: https://www.color-hex.com/ (accessed on 1 November 2019).



© 2020 by the authors. Licensee MDPI, Basel, Switzerland. This article is an open access article distributed under the terms and conditions of the Creative Commons Attribution (CC BY) license (http://creativecommons.org/licenses/by/4.0/).